Ionization of He atoms during grazing scattering from a metal surface

S. Wethekam,[1] H. Winter,[1] Diego Valdés,[2] and R. C. Monreal[2,*]
[1]*Institut für Physik, Humboldt-Universität zu Berlin, Newtonstr. 15, D-12489 Berlin, Germany*
[2]*Departamento de Física Teórica de la Materia Condensada C-V, Universidad Autónoma de Madrid, E-28049 Madrid, Spain*
(Received 16 February 2009; revised manuscript received 13 April 2009; published 8 May 2009)

We present a theoretical analysis of experimental data on ion fractions and polar angular distributions for He atoms and ions produced during grazing scattering of keV neutral He atoms from an atomically clean and flat Al(111) surface. The discussion focuses on the mechanism of Auger ionization for which we have recently presented the first quantitative treatment by an *ab initio* method [S. Wethekam, Diego Valdés, R. C. Monreal, and H. Winter, Phys. Rev. B **78**, 033105 (2008)]. Auger ionization, the inverse process of Auger neutralization, is a dynamical process that converts kinetic energy from the projectile to electronic excitations. We calculate Auger ionization rates and perform molecular-dynamics and Monte Carlo simulations of trajectory and charge state of scattered projectiles. We achieve quantitative agreement with experimental ion fractions and angular distributions. This demonstrates that Auger ionization is an efficient mechanism of ionization. We also discuss the sensitivity of the results on the theoretical input used in the simulations and give an estimate on the contribution of resonant processes.

DOI: 10.1103/PhysRevB.79.195408 PACS number(s): 79.20.Rf, 79.60.Bm, 61.85.+p

I. INTRODUCTION

Charge transfer reactions between atomic particles and metal surfaces are important processes in different fields of physics and chemistry. The two basic mechanisms of charge transfer are named resonant electron transfer and Auger electron transfer. The binding energy of the atom and the electronic structure of the surface determine the dominant mechanism. The interaction of particles of low binding energy as, e.g., alkali atoms, with metal surfaces has been extensively studied experimentally and is well understood theoretically on the basis of the one-electron resonant mechanism.[1–8] However, a similar degree of understanding has not been achieved so far concerning reactions for atoms of higher electronic binding energy. This is largely due to the fact that here charge transfer proceeds via two-electron Auger processes.[2,9,10] In Auger neutralization (AN), a metal electron neutralizes the ion with the excess energy and momentum being transferred to another metal electron or a plasmon. In the inverse process of Auger ionization (AI), an electron bound to the projectile is excited to an unoccupied state of the metal accompanied by excitation of another metal electron or a plasmon.[2,11–13] The particle velocity sets a fundamental limit between these two types of Auger processes. AN can operate as long as the atomic level is below the Fermi level also for the atom at rest, while AI requires a minimum of kinetic energy of the projectile to excite the electronic system.

The problem of charge transfer between noble gas ions/atoms and metal surfaces has received attention for a long time.[9] In this respect, He/Al is considered as a model system since He is the simplest noble gas atom and Al is the prototype of a nearly-free-electron metal.[10] In spite of its apparent simplicity, a microscopic understanding of the AN process has only been achieved recently. Experimental findings[9,14–27,36] and theoretical calculations of AN rates[28–33] are in accord only if the atomic energy level is substantially modified near the surface.[4,17,19,23,25,32,34–37] These former theoretical and experimental efforts were focused on the understanding of the AN process at low energies where reionization[2,11–13,18,26,38] can be generally neglected and the ion fractions result from an incomplete neutralization of the incident ions.[20,21,36] This understanding allows us to address the inverse problem of AI. Earlier experimental results on the ionization of neutral atoms[12,13] seemed to agree with theoretical estimates[11] for the existence of a kinetic energy threshold below which AI is forbidden, but a full theory is still lacking.

This paper is devoted to the study of the Auger ionization process. We will give theoretical and experimental evidence that AI is an efficient contribution to charge transfer for the system He/Al for small perpendicular velocities with a threshold in parallel energy of 4–5 keV. A preliminary study was published in Ref. 39. We find that the Auger ionization process is closely related to collisions of projectiles with thermally displaced target atoms, which gives a characteristic time scale for the ionization process on the order of some 10 as. As the neutralization mechanism for this system [He^+-Al(111)] is understood on a quantitative level,[36] this yields the interesting opportunity to study the attosecond electron dynamics[40] of the ionization process under well-defined conditions. Aside from fundamental aspects, our work may contribute to the understanding of collision cascades for keV atoms in solids, where the production of hot electrons in close collisions is a relevant mechanism of energy dissipation.[41]

The article is organized as follows. Section II describes the experimental techniques. The theory for Auger ionization is expounded in Sec. III A, where we show that the AI rate depends exponentially on distance between projectile and surface; energy level and projectile velocity. In Sec. III B, we summarize the rest of the theoretical input to be included in the molecular-dynamics and Monte Carlo simulations of ion fractions and polar angular distributions of scattered particles for comparison with our experiments. Comparison of theory and experiment is made in Sec. IV. We show in Sec. IV A that the calculations reproduce the observed kinetic energy

threshold, the overall magnitude of the ion fractions, and their increase with energy. The polar angular distributions for scattered ions and neutrals are also reproduced on a quantitative level (Sec. IV B). In our analysis, we find that a sufficiently large number of the incident neutrals reach distances to the surface where the He-1*s* level has been promoted and efficient AI is present. We also estimate the role of resonant processes in Sec. V. Using a simple model, we find these processes to be as important as the Auger effect. The role of the interaction potentials and lattice vibrations on the polar angular distributions is analyzed in Sec. VI. Section VII presents results where we combine Auger and resonant processes. Finally, we conclude in Sec. VIII that AN *and* AI have to be included for the quantitative description of charge transfer between noble gas atoms and metal surfaces under grazing scattering conditions.

In our analysis, we make use of concepts and results presented in Refs. 32 and 36, which are only briefly discussed here. The reader is referred to our previous works for more details. Atomic units (a.u.) ($e=\hbar=m=1$) are used if not otherwise stated.

II. EXPERIMENTS

In our experiments, we have scattered $^4He^0$ atoms with energies E of 1–11 keV under grazing angles of incidence Φ_{in} of typically 2° along high-index ("random") directions from an atomically clean and flat Al(111) surface. After dispersion with respect to charge in an electric field, scattered projectiles were detected using a position-sensitive microchannel plate detector. A simple sketch of the essential components of the experimental setup is shown in the inset of Fig. 2.

The target was prepared by cycles of grazing sputtering with 25 keV Ar^+ ions and subsequent annealing at 430 °C for about 10 min. The morphology of the surface was monitored by recording angular distributions for grazingly scattered atoms. Due to the long trajectories for this extreme geometry, the shape of angular distributions is extremely sensitive to surface defects.[42] From the absence of pronounced tails, we conclude from simulated angular distributions (see below) a high quality of the Al(111) surface widely free from defects. For a more detailed discussion of the experimental techniques, we refer to Ref. 36.

For grazing incidence, scattering proceeds in the surface channeling regime[2,43] where the projectiles are steered well above the topmost layer of the surface and the motions parallel and normal with respect to the surface are widely decoupled. The parallel motion takes place with nearly constant velocity such that the energy can be decomposed into a parallel and a normal part: $E=E_{\|}+E_{\perp}$, with $E_{\|}=E\cos^2\Phi_{in}$. The effective energy for impact onto the surface is given by the normal incident energy $E_{\perp}^{in}=E\sin^2\Phi_{in}$ which is on the order of eV for keV projectiles and $\Phi_{in}\sim 2°$.

III. THEORY

In this section, we present the theoretical ingredients for the calculation of ion fractions and polar angular distributions for scattered projectiles that will be compared to our experiments. The most recent aspect of this work is the theory of the Auger ionization rate expounded in subsection A. In subsection B, we summarize the further theoretical input for the simulations.

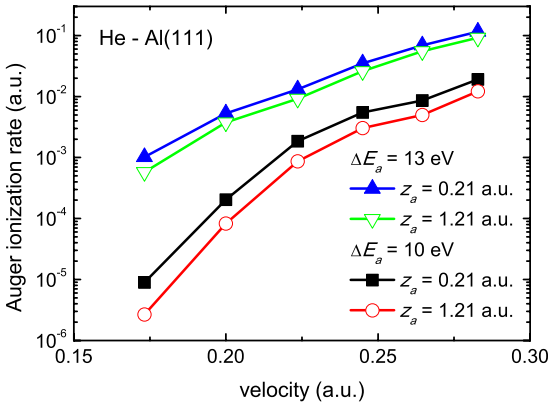

FIG. 1. (Color online) Auger ionization rate as function of projectile velocity for two values of energy level of He (shifted by $\Delta E_a=10$ and 13 eV with respect to its unperturbed value in vacuum) and distances to topmost surface layer $z_a=0.21$ a.u. and $z_a=1.21$ a.u.

A. Auger ionization rate

The theory for Auger ionization follows closely that of Auger neutralization since both processes are inverse to each other. Using a simple electronic model of a metal surface (jellium model), the transition rate for AN can be calculated,[29,30] including one-electron and multielectron (plasmon) channels. For AI, we follow a similar approach, however, incorporating the kinetic energy of the projectile. In the jellium model, electronic surface wave functions are translationally invariant which simplifies the treatment of Auger ionization mathematically. The generalization of the approach presented here to cases where molecular orbitals can be formed is deferred to a future study. For grazing incidence experiments, one has a projectile motion parallel to the surface with velocity $\mathbf{v}$ and perpendicular distance z_a. As reference, distances are measured with respect to the first atomic layer of Al, with the jellium edge for Al(111) at 2.21 a.u. Energies of electronic states are referred to the bottom of the conduction band.

In the restframe of the solid, the initial state of the electron bound to the atom is written as

$$|\Phi_a\rangle = \phi_a(\mathbf{x}-\mathbf{v}t, z-z_a)e^{i\mathbf{x}\cdot\mathbf{v}}e^{-i(E_a+(1/2)v^2)t}, \qquad (1)$$

with $\phi_a(\mathbf{x},z)$ being the wave function of the bound electron in the restframe of the ion, $(\mathbf{x},z)$ being the electron coordinates parallel and perpendicular to the surface, respectively, and E_a being the electron binding energy. Equation (1) includes the translation factor $e^{i\mathbf{x}\cdot\mathbf{v}}$ as well as the additional kinetic energy $v^2/2$ of the electron. The final state of this electron is an unoccupied state of the conduction band of the metal

$$|\mathbf{k}\rangle = \frac{1}{\sqrt{2\pi}} e^{i\mathbf{k}_\parallel \cdot \mathbf{x}} \psi_{k_z}(z) e^{-iE_\mathbf{k} t}, \tag{2}$$

with electron wave vector $\mathbf{k}=(\mathbf{k}_\parallel, k_z)$ and energy $E_\mathbf{k}=k^2/2$. The electron-electron Coulomb interaction $\hat{V}$ causes at the same time the excitation of the metal from its many-body ground state $|0\rangle$, energy E_0, to a state $|n\rangle$ of energy E_n. The matrix elements for the process are

$$\langle f|\hat{V}|i\rangle = \int \frac{d\mathbf{q}}{(2\pi)^2} \int dz_1 \langle n|\delta\hat{n}(\mathbf{q},z_1)|0\rangle \frac{2\pi}{q} \langle \mathbf{k}|^{i\mathbf{q}\cdot\mathbf{x}} e^{-q|z-z_1|} |\Phi_a\rangle. \tag{3}$$

In Eq. (3), $\langle n|\delta\hat{n}(\mathbf{q},z_1)|0\rangle$ are the matrix elements of the charge-density operator of the metal surface. A Fourier transform in the coordinates $\mathbf{x}$ parallel to the surface has been performed, with $\mathbf{q}$ being the corresponding wave vector. Due to the translational invariance of the metal surface, the time dependence of the matrix elements can be factored out completely as $e^{-i[E_0-E_n+E_a-v^2/2-E_\mathbf{k}+(\mathbf{k}_\parallel-\mathbf{q})\cdot\mathbf{v}]t}$, which allows us to make use of Fermi's golden rule and write down the transition rate for the process as

$$\frac{1}{\tau_{\mathrm{AI}}} = 2\pi \sum_n \sum_{k>k_F} \int_0^\infty d\omega |\langle f|\hat{V}|i\rangle|^2 \delta[\omega - (E_n - E_0)] \times \delta[-\omega + E_a - v^2/2 - E_\mathbf{k} + (\mathbf{k}_\parallel - \mathbf{q})\cdot\mathbf{v}], \tag{4}$$

with k_F being the Fermi wave vector and $\langle f|\hat{V}|i\rangle$ denoting here the spatial part of Eq. (3). The sum over excited states $|n\rangle$ can be related to the imaginary part of the dielectric susceptibility of the metal surface $\chi(\omega,q;z_1,z_2)$. The Galilean transformation $\mathbf{k}\to\mathbf{k}+\mathbf{v}$ yields our final expression for the Auger ionization rate as follows:

$$\frac{1}{\tau_{\mathrm{AI}}}(\mathbf{v},z_a,E_a) = 2 \sum_{|\mathbf{k}+\mathbf{v}|>k_F} \int_0^\infty d\omega \int \frac{d\mathbf{q}}{(2\pi)^2} \int dz_1 \int dz_2 [-\mathrm{Im}\ \chi(\omega,q;z_1,z_2)] V(\mathbf{k};\mathbf{q},z_1) V^*(\mathbf{k};\mathbf{q},z_2) \delta(E_a - E_k - \omega - \mathbf{q}\cdot\mathbf{v}), \tag{5}$$

where

$$V(\mathbf{k};\mathbf{q},z) = \frac{2\pi}{q} \langle \mathbf{k}|e^{i\mathbf{q}\cdot\mathbf{x}'} e^{-q|z'-z|} |\phi_a(\mathbf{x}', z'-z_a)\rangle. \tag{6}$$

The states $|\mathbf{k}\rangle$ and $|\phi_a(\mathbf{x}', z'-z_a)\rangle$ are required to be orthogonal to each other. We use the orthogonalized plane wave method (OPW) and orthogonalize $|\mathbf{k}\rangle$ [cf. Eq. (2)] to the atomic wave function $|\phi_a(\mathbf{x}', z'-z_a)\rangle$, which we take as the Hartree-Fock one for the He atom. Then, the matrix elements given by Eq. (6) are obtained by integration in the coordinates $(\mathbf{x}', z')$.

In Eq. (5), energy conservation implies that frequency and wave vector are related via the Doppler relation $\omega'=\omega+\mathbf{q}\cdot\mathbf{v}$. As a consequence, different from previous assumptions,[2,11–13] there is no clear-cut threshold for the kinetic energy of the projectile below which the AI process is energetically forbidden. Rather, the δ function of Eq. (5) can be used to give the cosine of the angle between vectors $\mathbf{q}$ and $\mathbf{v}$ and, therefore, imposes the constraint

$$-1 \le \frac{E_a - E_\mathbf{k} - \omega}{qv} \le 1. \tag{7}$$

The bound electron has to be excited to an empty state of the shifted Fermi sphere so that

$$\frac{1}{2}(k_F - v)^2 \le E_\mathbf{k}. \tag{8}$$

Equations (7) and (8) and the condition $\omega \ge 0$ yield a lower limit for q as follows:

$$q \ge \frac{\frac{1}{2}(k_F - v)^2 - E_a}{v}. \tag{9}$$

Then, for small v or negative E_a with large modulus, the allowed values of the parallel wave vector q will be much larger than k_F. However, the surface response function strongly disfavors excitations of large wave vectors and, consequently, the efficiency of the Auger ionization process can be very small. This is illustrated in Fig. 1, where we plot Auger ionization rates for He in front of Al as a function of the projectile velocity for two values of the energy-level shift ΔE_a of the $1s$ level of He. Instead of a thresholdlike behavior, the AI rates show an overall exponential increase with velocity. We also find an exponential increase with E_a (see Fig. 2 of Ref. 39). However, the increase is steeper for smaller values of velocity and E_a, as expected from our discussion above. We showed in Ref. 39 that the AI rate is nearly exponentially decreasing with distance. Here, we present results for two distances illustrating that the spatial decay length depends mainly on E_a and it is less dependent on velocity or distance (only indirectly via variation of E_a) since, for a given E_a, the curves for different z_a are nearly parallel. Note also in this figure that the AI rates can become quite large. As a reference, the calculated AN rates for He/Al are about 0.01–0.02 a.u. at the distances shown in Fig. 1. Then efficient Auger ionization is expected for neutral He atoms with a velocity of about 0.25 a.u. closer than about 1 a.u. in front of the Al surface, where calculated values of E_a (Ref. 32) show level shifts greater than 10 eV. This will be demonstrated in Sec. IV.

B. Interaction potentials and energy levels of He in front of Al(111)

Theoretical[32,34,35,37] and experimentally[23] derived energy-level shifts $\Delta E_a(\mathbf{r})$ of the $1s$ level of He in front of Al(111) show pronounced variations close to the surface. $-\Delta E_a(\mathbf{r})$ represents the change in the ionization potential of the He atom at a position $\mathbf{r}$ in front of the surface with respect to its unperturbed value. As a consequence, the analysis of the experimental data requires detailed three-dimensional calculations of the trajectories for atoms/ions including charge transfer during their interaction with the surface, where the energy level varies along the trajectory.

The input of the simulations is as follows. The He^0-Al interaction $V_{He^0}(\mathbf{r})$ is described by the Molière potential with modified Firsov screening length as proposed by O'Connor and Biersack[44] (OCB). This potential reproduces in simulations the width and shape of experimental polar angular distributions of scattered neutral He. This aspect is relevant here as the width of angular distributions is determined by binary collisions with thermally displaced target atoms.[2,42,45] As ionization processes are closely related to the latter, their realistic reproduction in the simulations is of paramount importance. For a more detailed discussion on the choice of the He^0-Al interaction potential, we refer to Ref. 36. The interaction potential for charged projectiles $V_{He^+}(\mathbf{r})$ is constructed from the potential for neutrals reduced by the level shift $\Delta E_a(\mathbf{r})$,[2,10,23,34]

$$V_{He^+}(\mathbf{r}) = V_{He^0}(\mathbf{r}) - \Delta E_a(\mathbf{r}). \tag{10}$$

The analysis of the experimental data indicates that the range of distances for ionization of He^0 is about 0.5–1 a.u. from a surface atom. At these distances, strong hybridization between He and Al causes the formation of molecular orbitals. The strong variation in the He-$1s$ level shown in Ref. 32 stems from its interaction with the core $2s$ and $2p$ electrons of Al. As the calculated E_a corresponds to the on-top position, it is evaluated as function of distance to the closest target atom (with slight modifications to ensure continuity). Also as a consequence of hybridization, the matrix elements for charge transfer processes cannot be computed from unperturbed atomic wave functions but have to be corrected by the weight coefficient of He in the molecular orbital that approaches the pure He orbital at infinite distance between atom and surface.[46] The correction factor is about 0.6 for close He-Al distances and is included in the AI rates used.

Ions produced in the ionization process can be Auger neutralized on their way away from the surface. We use the Auger neutralization rate as calculated with a linear combination of atomic orbitals (LCAOs) method in Ref. 32 on a hollow position which reproduces the experimental fractions of surviving ions obtained for small incident energies[36] better than the jellium rates. Since the main difference between the jellium and LCAO calculations of AN in Ref. 32 is due to orthogonalization effects, we consistently correct the jellium rates for AI by the same factor that brings the rates for AN from the jellium to the LCAO values.

With the interaction potentials for ions and neutrals and the neutralization and ionization rates, we perform combined Monte Carlo and molecular-dynamics simulations of charge state and trajectory for scattered projectiles. The surface is represented by clusters of Al atoms centered below the projectile including correlated thermal displacements (for details we refer to Ref. 45). For each time step of the calculations, the Newton equations of motion for the projectile and the Al target atoms as well as the rate equation for electron capture or loss are solved using a fourth-order Runge-Kutta method. The charge state of the projectile after each step is determined by reference of the calculated average charge state (from the Runge-Kutta solution of the rate equation for capture or loss) to a random number. For each trajectory, the final charge state and exit angle are stored for comparison with measured charge fractions and angular distributions. The angular acceptance window used in the simulations is that of the experimental setup.

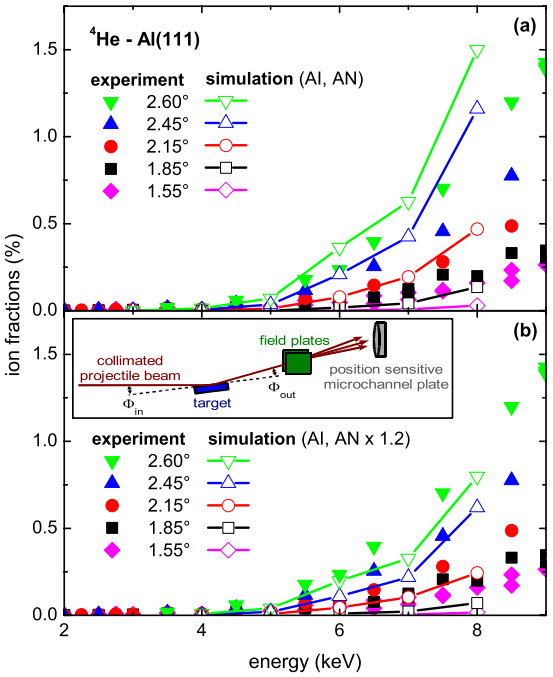

FIG. 2. (Color online) Ion fractions for scattering of $^4He^0$ atoms from Al(111) along high-indexed ("random") directions under grazing angles of incidence Φ_{in} indicated as function of energy E. Full symbols: experimental data; open symbols with curves: results from simulations including AN and AI processes for original rates (panel a) and for AN rates multiplied by a factor of 1.2 (panel b). Inset: simple sketch of experimental setup.

IV. RESULTS

A. Ion fractions

In Fig. 2(a), we compare ion fractions from our simulations as a function of beam energy E (curves with open symbols) with the experimental data (full symbols) for scattering of He^0 atoms from Al(111) under grazing angles of incidence indicated. In the simulations, we find that incident neutrals reach distances to the surface where the energy level of He has been substantially promoted and efficient Auger loss is present. The increase in the ion fractions with incident en-

ergy and angle is reproduced by the simulations on a quantitative level. The largest discrepancy between theory and experiment occurs at the largest calculated values of incident energy and angle of incidence. This could be due to a poorer description of the interaction potentials and energy-level variation close to the surface. The interaction potential determines the number of neutrals that reaches distances where efficient ionization can occur. This efficiency depends strongly on the values of E_a, as it is apparent from Fig. 1. We will discuss this point below. Another source of uncertainty is related to the accuracy of the calculated Auger neutralization rates due to theoretical approximations such as distinguishability of electrons and use of unperturbed metal wave functions. In our former analysis of ion fractions in the survival regime[36] calculated AN rates have to be increased by a factor of 1.2 in order to get perfect quantitative agreement between theory and experiment for Al(111).[47] Such a factor is within the estimated error of theory.[30,48] Its effect in the present experimental case is shown in Fig. 2(b) where the overall agreement with experiment is improved.

We attribute the discrepancy between experimental data and simulation for the smallest angles of incidence to surface defects. The role of surface defects for the ion fractions is expected to be most pronounced for long trajectories (small angles of incidence Φ_{in}, i.e., large probability to "hit" a surface defect) and low ionization efficiencies for the ideal surface (small "real" signal). Therefore, the increase in ion fractions with angle cannot be attributed to surface defects. In order to explain the experimental data for $\Phi_{in}=1.55°$, only a few percent of incident He^0 atoms have to undergo ionization at surface defects. For the typical length scale of about 2×1 a.u./sin $1.55° \approx 70$ a.u. of the trajectory close to the turning point, this is still in accord with a good quality of the surface. Moreover, collisions with surface defects can be identified by characteristically broadened angular distributions for outgoing ions. These are observed for ionized projectiles at the smallest angle of $\Phi_{in}=1.55°$ and for about half of the ions at $\Phi_{in}=1.85°$ but not for the larger angles. Whereas the influence of surface defects cannot be fully neglected for $\Phi_{in}=1.55°$ and $\Phi_{in}=1.85°$, our data at larger angles are not masked by surface defects (see also discussion in Sec. IV B).

In the simulations, we also obtain fractions $P_{ionized}$ of initially neutral projectiles that have been ionized at least once. These that survive Auger neutralization on their way out determine the ion fractions P^+ plotted in Fig. 2(a). The (averaged) Auger survival probability on the way out of the ionized projectiles is obtained as $P_{AN}^{+,out} \simeq P^+/P_{ionized}$ which represents an average value over the different trajectories [see Eq. (11) below]. $P_{ionized}$ and $P_{AN}^{+,out}$ are plotted in Fig. 3 as a function of the incident energy for several angles of incidence. The efficiency of the Auger ionization process can be inferred from this figure: the ionization probability increases with energy and angle up to 35%. The Auger survival probability on the way out is significantly smaller and shows much weaker variations. This is because this magnitude depends basically on the perpendicular outgoing velocity and the ionization distance z_{ion} in front of the surface via

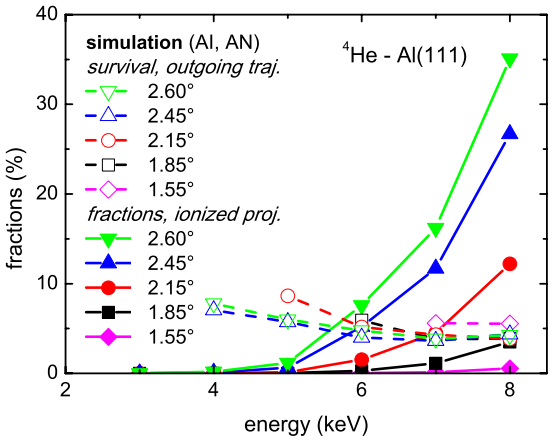

FIG. 3. (Color online) Full symbols with solid curves: fractions $P_{ionized}$ of initially neutral He projectiles that have been ionized at least once along trajectory. Open symbols with dashed curves: fractions $P_{AN}^{+,out}$ of ionized projectiles that are not neutralized by AN on outgoing trajectory. Results are shown as function of energy for scattering from Al(111) under angles of incidence Φ_{in} indicated.

$$P_{AN}^{+,out} = \exp\left(-\int_{z_{ion}}^{\infty} \frac{dz}{v_z \tau_{AN}(z)}\right), \tag{11}$$

where v_z and z_{ion} do not change much under the present experimental conditions, when averaged over the trajectories (see Figs. 4 and 5 below).

B. Polar angular distributions

Figure 4(a) shows experimental polar angular distributions (polar exit angle Φ_{out}) for outgoing He^0 atoms (open black circles) and He^+ ions (full red circles) produced during scattering of 7.5 keV neutral $^4He^0$ atoms from Al(111) under different grazing angles of incidence Φ_{in}. All distributions are normalized to 1 at their maximum. The distributions for outgoing ions are displaced from the distributions for outgoing neutrals toward larger exit angles. This fact is opposite to the effect of the classical image potential interaction between a charged particle and a metal surface where the charged particle would be attracted by its image and deflected toward smaller polar exit angles. Thus, this interaction has to be strongly modified by nonimagelike contributions. But, even for a strongly modified level shift in front of the surface, it would also be difficult to explain the shifts as the normal energy $E_{\perp}^{out}=E \sin^2 \Phi_{out}$ for the maxima of the distributions of outgoing ions is enhanced to about 15 eV with respect to the maxima of the distributions for outgoing neutral atoms. This value is too large to be consistent with a downward shift of the He-1s level.[32,36] Therefore, the shifts of the angular distributions may have their origin in the production of ions in close collisions and angle-dependent survival probabilities for ions along the outgoing trajectory.

For the smallest two angles of incidence, $\Phi_{in}=1.55°$ and $\Phi_{in}=1.85°$, the distributions for ions are broad so that surface steps and/or defects play an important role, responsible also for the long tail of the distributions extending to small exit angles. For the three largest angles, the angular distributions

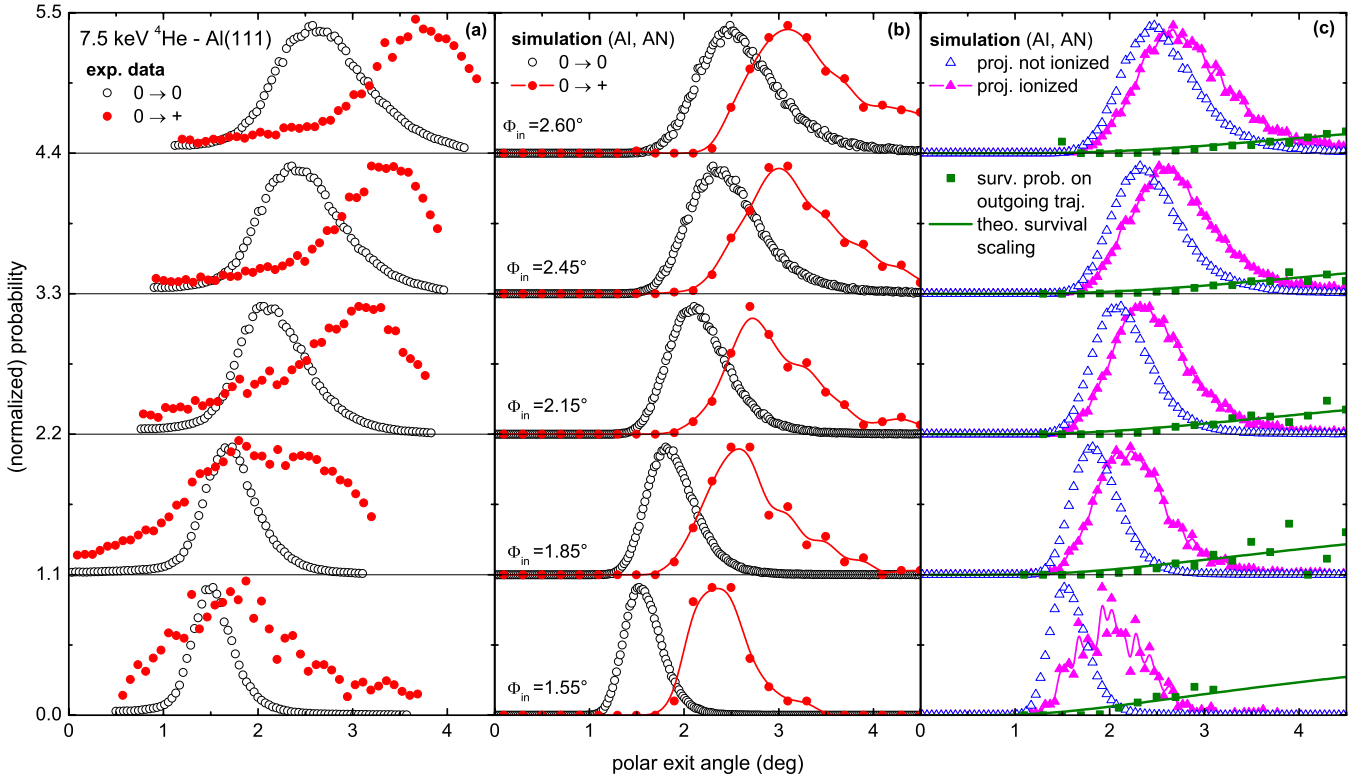

FIG. 4. (Color online) Panel a: experimental angular distributions as function of polar exit angle Φ_{out} for scattering of 7.5 keV $^4He^0$ atoms from Al(111) under angles of incidence as indicated. Open black circles (full red circles): outgoing atoms "0" (ions "+"). Panel b: simulated angular distributions for the same conditions based on AI and AN as charge transfer mechanisms. Panel c (same conditions): normalized angular distributions for projectiles that have never been ionized (blue open triangles) and projectiles that have been ionized at least once (magenta full triangles with solid curve). Ion survival probability $P_{AN}^{+,out}$ on the outgoing trajectory (full green squares) and theoretical scaling of $P_{AN}^{+,out}$ according to Eq. (12) as function of the exit angle. All distributions are normalized to 1. Data are offset by multiples of 1.1.

are well defined and in good accord with our trajectory simulations, which indicates a minor role of surface defects. We conclude that for $\Phi_{in} > 1.85°$, surface defects can be neglected for ion fractions and angular distributions.

The results of the simulations are plotted in Fig. 4(b). While the distributions for neutrals (black open circles) are well reproduced, the agreement for the distributions for ions (full red circles with solid red curves) with the experimental data is poorer. The discrepancy in the region of small polar angles can be attributed to defects. The simulations reproduce the displacement of the angular distributions toward larger polar angles for scattered ions. However, the simulated distributions peak at too small values of the polar exit angle, with the differences being larger for larger angles of incidence. The discrepancy at large angles of incidence was already noted in the analysis of the ion fractions and is ascribed to deficiencies in the interactions potentials, which become more important for closer distances of approach between He and Al atoms. In order to understand the physical origin of the angular displacement, we plot in Fig. 4(c) simulated distributions for projectiles that have never been ionized (open blue triangles) for ionized projectiles $P_{ionized}$ (full magenta triangles) and, from its ratio to P^+, the dependence with the polar exit angle of the (average) Auger survival probability on the outgoing trajectories $P_{AN}^{+,out}$ (full green squares). $P_{AN}^{+,out}$ can be written as a function of the polar exit angle Φ_{out} by noting that, for the small values of Φ_{out}, $v_\perp = v \sin(\Phi_{out}) \simeq v\Phi_{out}$ so that [cf. Eq. (11)]

$$P_{AN}^{+,out}(\Phi_{out}) \simeq \exp[-\alpha/\Phi_{out}], \tag{12}$$

where α is a constant. This function is also plotted in Fig. 4(c) (solid green curve) and shows that the simulated $P_{AN}^{+,out}$ follows the theoretically expected behavior of increase with Φ_{out}. On the other hand, the distribution of the ionized projectiles is peaked, decreasing for large outgoing angles. Then, the competition between the opposite trends of $P_{ionized}$ and $P_{AN}^{+,out}$ with Φ_{out} determines the final shape of the distribution for outgoing ions. Note also in Fig. 4(c) that $P_{ionized}$ is displaced toward larger polar exit angles with respect to the distribution of projectiles that always remain neutrals. This indicates that the ionization process has occurred in close collisions with Al atoms and a corresponding deflection of ions toward larger exit angles.

In Fig. 5, we show simulated distributions for the projectiles that have not been ionized (open blue triangles), the ionized projectiles (full magenta triangles), and the total number of projectiles (solid black curve) as a function of the minimum distance of approach to a target atom. In this figure, the distributions are normalized so that they give the calculated ion fractions. Those incident neutral atoms that reach distances shorter than about 1.1 a.u. are ionized in the

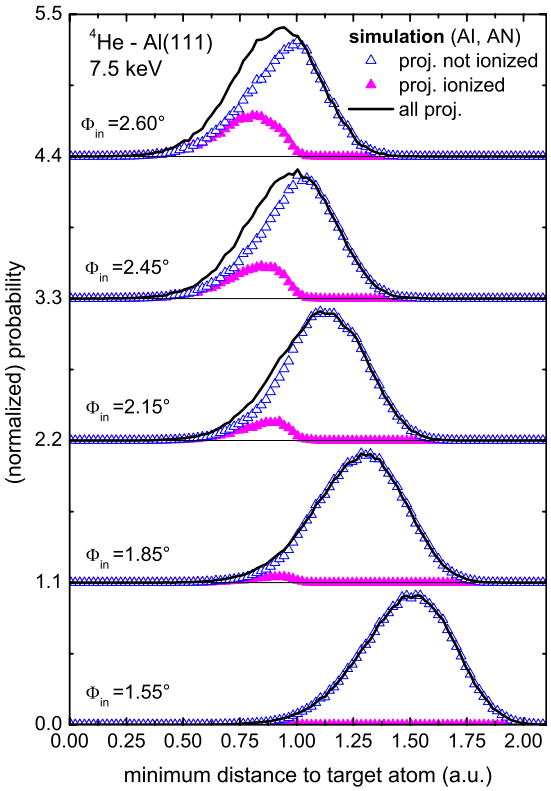

FIG. 5. (Color online) Simulated (for charge transfer mechanisms AI and AN) distributions as function of minimum distance to a target atom for: all projectiles (black solid curve), projectiles that have not been ionized (blue open triangles), and projectiles that have been ionized (magenta full triangles). The incident energy of $^4He^0$ atoms is 7.5 keV at grazing angles of incidence as indicated. The maxima of distributions for all projectiles are normalized to one and other distributions are normalized to give the correct ion fractions. Results for different angles of incidence offset by multiples of 1.1.

close collision with appreciable probability on a time scale of about $t_{\text{ion}} \simeq \frac{0.5}{0.3}$a.u. $\simeq 40$ as. At these distances, the promotion of the He-1s level is large enough to make the Auger process an efficient mechanism for ionization for kinetic energies larger than 5 keV. Since the interaction potentials and the lattice vibrations determine the distribution in distances of closest approach of the incident particles, they are crucial parameters, together with the ionization and neutralization rates, for simulated ion fractions and polar distributions. We will address this issue in Sec. VI.

V. ROLE OF RESONANT PROCESSES

As shown in Fig. 5, He^+ ions are produced at distances smaller than 1.1 a.u. to a target atom where the promoted He level overlaps with the conduction band and, consequently, resonant processes cannot be excluded. In this range of distances, the strong hybridization between He and Al would require a full quantum calculation for these processes which is outside the scope of the present work. A semiclassical calculation is used here to calculate the rates for resonant neutralization and resonant ionization.

In general, the level width $\Gamma(E_a, z_a)$ of an atomic level of energy E_a interacting with a continuum of states at a distance z_a is defined as the imaginary part of its self-energy,

$$\Gamma(E_a, z_a) = -2\ \text{Im} \sum_k T_k^2(z_a) \frac{1}{E_a - \epsilon_k + i\eta}, \tag{13}$$

where $T_k(z_a)$ are the hopping matrix elements between the atom and the continuum of k states of energy ϵ_k and η is an infinitesimal. We now assume that the matrix elements depend only on energy and change Σ_k by $\int d\epsilon \rho(\epsilon)$, with $\rho(\epsilon)$ being the density of states. The densities of states and the hopping matrix elements can also be expressed in a local basis of 3s and 3p states for the case of Al. Figure 1a of Ref. 35 shows the hopping matrix elements between He and Al, where the hopping with the 3pz orbital goes to zero for the distances shorter than 1 a.u. Moreover, the total charge of this orbital is small (0.15 electrons) in comparison with the one of the 3s orbital (0.89 electrons). Then, keeping only the contribution of the 3s orbital of Al to the level width, we have

$$\Gamma(E_a, z_a) = 2\pi \rho_{3s}(E_a) |T_{3s}(z_a)|^2. \tag{14}$$

The rates for resonant neutralization (RN) and ionization (RI) are obtained from Eq. (14) as[3]

$$\frac{1}{\tau_{\text{RN}}}(E_a, z_a) = g_c f_{\text{FD}}(E_a, v) \Gamma(E_a, z_a) \tag{15}$$

and

$$\frac{1}{\tau_{\text{RI}}}(E_a, z_a) = g_l (1 - f_{\text{FD}}(E_a, v)) \Gamma(E_a, z_a), \tag{16}$$

respectively. $f_{\text{FD}}(\epsilon, v)$ is the Fermi-Dirac distribution function modified by the parallel velocity[2,3,11] and $g_c = 1$ and $g_l = 2$ are the statistical spin factors for capture and loss[2,11] of one electron by He^+ and He^0, respectively. We assume a constant density of states containing 0.89 electrons up to the Fermi level. We have checked that this simple model reproduces the magnitude and the trends with projectile energy of the full quantum calculations of the ion fractions of Refs. 35 and 46 if we use $g_c = g_l = 1$ as it is appropriate for a comparison with those spinless calculations. We think that our approximation will give the order of magnitude of the ion fractions in the present case.

The resonant rates are plotted in Fig. 6 for parallel energies of 4 and 8 keV. The rates have been calculated using Eqs. (15) and (16) up to the distance of 0.75 a.u. and saturated for shorter distances. This is because, for $z_a \leq 0.75$ a.u., the values of E_a are such that the calculated densities of 3s and 3p states and, consequently, the resonant ionization rate go to zero. This kind of behavior does not seem realistic, and actually it would not occur if higher Al states would be included in our theory or in a free-electron description of the conduction band. We consider the saturation of the rate to be a reasonable approximation. Comparing the resonant ionization rate with the Auger rate of Fig. 1 for 8 keV, we note that the resonant rate is typically a factor of 2 larger than the Auger rate at short distances. However, the resonant rate goes to zero as soon as the He level is below

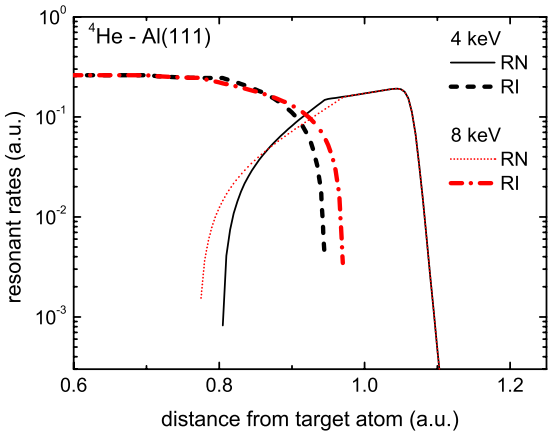

FIG. 6. (Color online) RN (thin solid black curve and thin dotted red curve) and RI (thick dashed black curve and thick dash-dotted red curve) rates as function of distance from a target atom for energies E=4 keV (thin solid black curve and thick dashed black curve) and E=8 keV (thin dotted red curve and thick dash-dotted red curve).

the Fermi level. On the other hand, the resonant rates depend weakly on projectile velocity (except for the small range of distances where the He-1s level crosses the Fermi level) while the Auger ionization rate depends exponentially on velocity. These differences produce the differences in our calculated ion fractions considering Auger or resonant processes at the smaller energies and angles of incidence.

The simulated ion fractions due to resonant processes are plotted in Fig. 7 together with the experimental results. We see that this order-of-magnitude calculation reproduces the experimental trends even though it tends to overestimate the increase in the ion fractions with angle of incidence. We thus conclude that Auger and resonant processes are equally important for ionization of He on Al(111). The simulated polar angular distributions are not very different to the ones shown in Figs. 4(b) and 5 obtained for Auger processes as in both cases ions are produced under similar conditions, i.e., in

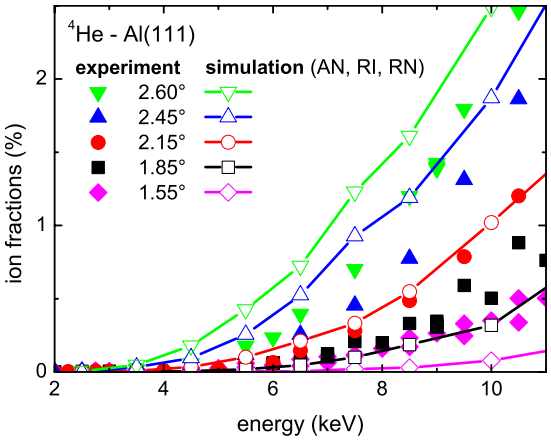

FIG. 7. (Color online) Ion fractions as function of energy for scattering of ^{4}He^0 from Al(111) under grazing angles of incidence indicated. Full symbols: experimental results; open symbols with curves: simulation including AN, RI, and RN as charge transfer mechanisms.

close collisions with thermally displaced target atoms.

In this work, we are basically interested in the ionization process of He^0, initially in its ground state. We estimate the rates for the resonant neutralization/ionization to the 1s state of He as competing with Auger processes to the same state. Once He$^+$ is formed, resonant as well as Auger charge transfer can occur to excited states due to the large parallel velocity of the projectile. These processes might also play a role in the measured ion fractions. However, the large spatial extent of the excited states makes it even more difficult to describe its interaction with the metal surface, and we do not attempt any estimation of its contribution here.

VI. ROLE OF INTERACTION POTENTIAL AND LATTICE VIBRATIONS

Figure 8, shows simulated polar angular distributions of neutrals and ions for incident ^{4}He^0 scattered from Al(111) with E=7.5 keV and Φ_{in}=2.15°, obtained by changing the screening length of the OCB potential or the rms (root-mean-square) amplitude of the thermal displacements by ±20%. All the distributions have been normalized to 1 at their maximum. Panels a and b present results using Auger and resonant processes, respectively. As we have anticipated, the parameters defining the interaction potentials have a major influence on the widths and the position of the maximum of the distributions, independent of the mechanism of charge transfer, since both operate essentially in the same range of distances.[49] The respective ion fractions as a function of energy are shown in panels c and d. As expected, the ion fractions increase (decrease) if the probability for close collisions with thermally displaced target atoms is increased (decreased) by weakening (strengthening) the potential or enhancing (reducing) the amplitude of thermal vibrations.

VII. COMBINED TREATMENT OF AUGER AND RESONANT PROCESSES

In Fig. 9, we summarize our main findings. Figure 9(a) shows ion fractions resulting from a calculation that includes Auger and resonant processes. These present very much the same characteristics already discussed. In Fig. 9(b), we present the same results but with the Auger neutralization rate multiplied by the factor of 1.2 mentioned above. The remarkable agreement between theory and experiment should not be overestimated in view of the limitations and approximations of the theory. A more refined and realistic theory should be based on improved calculations of interaction potentials, level shifts, thermal displacements, and transition rates including Auger ionization and neutralization as well as resonant processes for a quantitative description of charge transfer.

A better control of the relative contributions of Auger and resonant ionization processes could be achieved using metal surfaces with a larger threshold energy for RI as, e.g., Cu or Ag.[18,26,38] Under the present experimental conditions, this may result in a dominance of the AI process; however, the electronic structure of the surface is more complex. An option is the use of different isotopes of He for a controlled

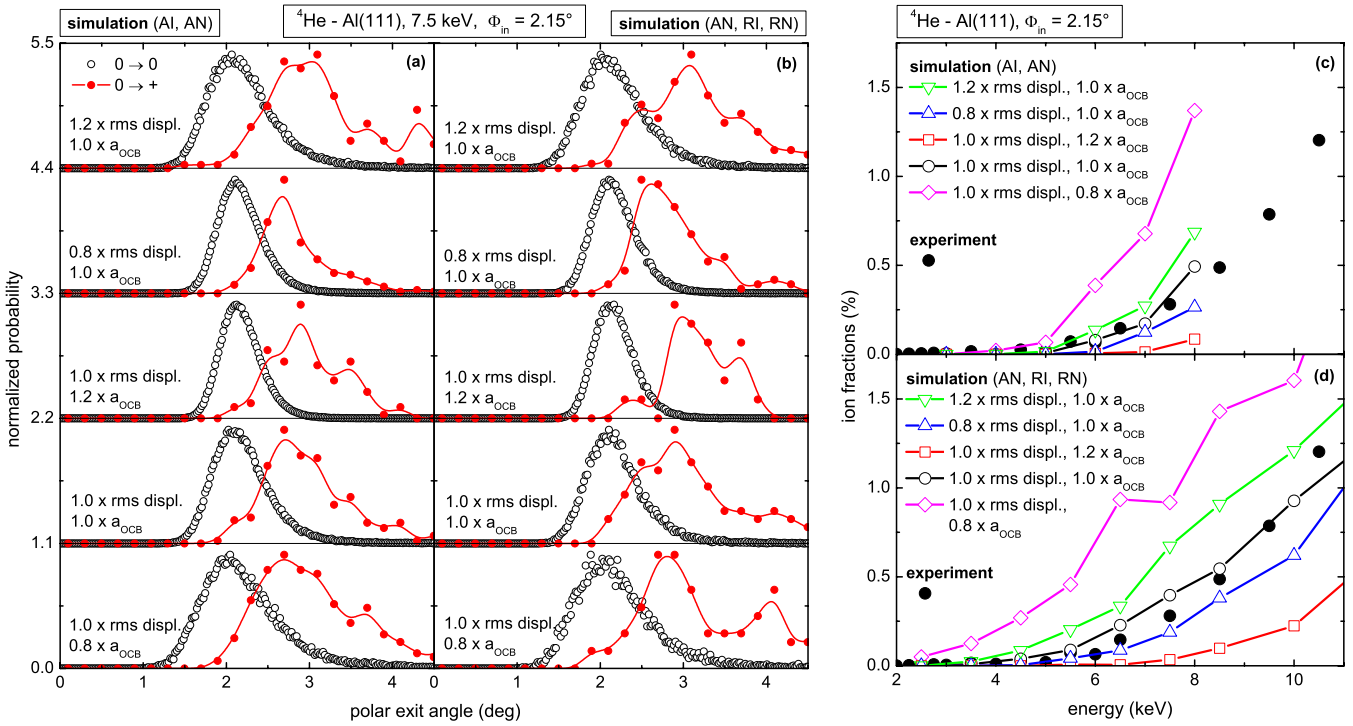

FIG. 8. (Color online) Simulated polar angular distributions for outgoing ions and neutrals (panels a and b, E=7.5 keV) and ion fractions as function of energy (panels c and d) for scattering of $^4He^0$ atoms under Φ_{in}=2.15° from Al(111). 1.2/1.0/0.8×rms displ.: rms amplitudes of thermal displacements multiplied by 1.2/1.0/0.8. 1.2/1.0/0.8×a_{OCB}: screening length of the OCB potential (Ref. 44) multiplied by 1.2/1.0/0.8. Different results are offset by multiples of 1.1.

variation in the projectile velocity for the same trajectories (same interaction potential for isotopes). Changes in velocity affect the AI but almost not the RI rates. This may allow one to isolate the contribution to ionization of the AI process. A suppression of the AI process can be achieved for heavier noble gas atoms (Ne) due to the reduced velocities at the same energies.

VIII. CONCLUSIONS

In this work, we have analyzed experimental data on ion fractions and polar angular distributions of scattered ions and neutrals, produced in the ionization process of neutral He impinging at grazing angles on Al(111), with energy of several keV. Our analysis focuses on the previously ignored mechanism of Auger ionization. We first calculate the rate for this process and find a nearly exponential dependence on velocity, energy level, and distance to the surface. From molecular-dynamics and Monte Carlo simulations of projectile trajectory and charge state, this process turns out to be an efficient mechanism of ionization, yielding threshold behavior and angular dependencies of ion fractions in quantitative agreement with experiments. The simulations show that Auger ionization occurs efficiently in a range of distances where resonant processes can also be operative. We estimate the contributions of these processes in a simple model and find both equally important. We also analyze the effect of the interaction potentials and lattice vibrations, which are responsible for the probability for close collisions with target atoms and the shape of the angular distributions. Excellent

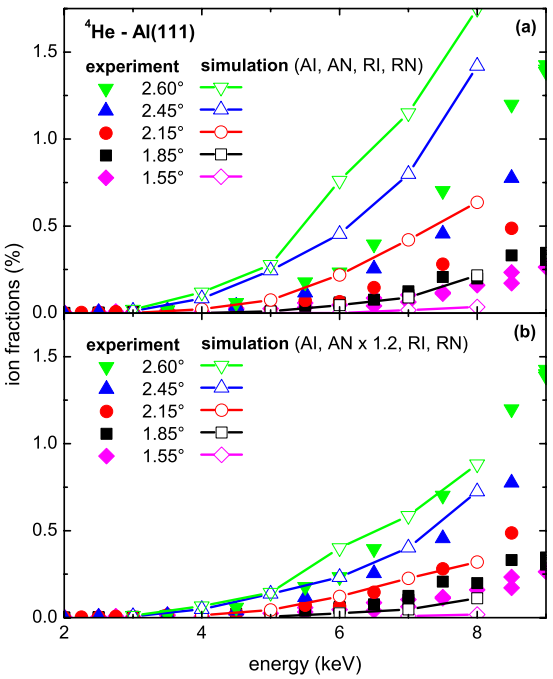

FIG. 9. (Color online) Ion fractions as function of energy for scattering of $^4He^0$ under grazing angles of indicated from Al(111). Full symbols: experimental data; open symbols with curves: simulations. Panel a: theoretical simulations including all charge transfer processes (AI, AN, RI, and RN) with original theoretical rates. Panel b: same as panel a but AN rate increased by a factor of 1.2.

agreement between measured and simulated ion fractions is obtained if we include resonant and Auger processes and, in addition, multiply the Auger neutralization rate by a factor of 1.2. This factor, which is within the estimated error of the theory, was previously found in our analysis of ion survival. We conclude that a realistic description of charge transfer between He and metal surfaces should include Auger ionization as well as Auger neutralization and resonant processes. In particular, the process of Auger ionization should be considered as one of the possible mechanisms involved in the so-called collision induced ionization/neutralization regime of atom-solid interactions.[18,26,38,41]

ACKNOWLEDGMENTS

We thank the DFG (Project No. Wi 1336) and the Spanish Ministerio de Educación y Ciencia (Project No. FIS2005-02909) for financial support and G. Adamov, K. Maass, A. Mertens, and A. Schüller for their assistance in the experiments.

*Author to whom correspondence should be addressed; r.c.monreal@uam.es

[1] J. Los and J. J. C. Geerlings, Phys. Rep. **190**, 133 (1990).
[2] H. Winter, Phys. Rep. **367**, 387 (2002).
[3] J. P. Gauyacq, A. G. Borisov, and M. Bauer, Prog. Surf. Sci. **82**, 244 (2007).
[4] J. Merino and J. B. Marston, Phys. Rev. B **58**, 6982 (1998).
[5] J. B. Marston, D. R. Andersson, E. R. Behringer, B. H. Cooper, C. A. DiRubio, G. A. Kimmel, and C. Richardson, Phys. Rev. B **48**, 7809 (1993).
[6] E. R. Behringer, D. R. Andersson, B. H. Cooper, and J. B. Marston, Phys. Rev. B **54**, 14765 (1996).
[7] J. Powers, J. R. Manson, C. E. Sosolik, J. R. Hampton, A. C. Lavery, and B. H. Cooper, Phys. Rev. B **70**, 115413 (2004).
[8] K. Niedfeldt, E. A. Carter, and P. Nordlander, J. Chem. Phys. **121**, 3751 (2004).
[9] H. D. Hagstrum, Phys. Rev. **96**, 336 (1954).
[10] R. C. Monreal and F. Flores, Adv. Quantum Chem. **45**, 175 (2004).
[11] R. Zimny and Z. L. Miskovic, Nucl. Instrum. Methods Phys. Res. B **58**, 387 (1991).
[12] H. Winter, G. Siekmann, H. W. Ortjohann, J. C. Poizat, and J. Remillieux, Nucl. Instrum. Methods Phys. Res. B **135**, 372 (1998).
[13] S. Wethekam, A. Mertens, and H. Winter, Nucl. Instrum. Methods Phys. Res. B **203**, 57 (2003).
[14] J. Roussel, C. Boiziau, R. Nuvolone, and C. Reynaud, Surf. Sci. **110**, L634 (1981).
[15] W. Sesselmann, B. Woratschek, J. Küppers, G. Ertl, and H. Haberland, Phys. Rev. B **35**, 1547 (1987).
[16] T. Hecht, H. Winter, and A. G. Borisov, Surf. Sci. **406**, L607 (1998).
[17] B. van Someren, P. A. Zeijlmans van Emmichoven, and A. Niehaus, Phys. Rev. A **61**, 022902 (2000).
[18] M. Draxler, R. Gruber, H. H. Brongersma, and P. Bauer, Phys. Rev. Lett. **89**, 263201 (2002).
[19] J. C. Lancaster, F. J. Kontur, G. K. Walters, and F. B. Dunning, Phys. Rev. B **67**, 115413 (2003).
[20] S. Wethekam, A. Mertens, and H. Winter, Phys. Rev. Lett. **90**, 037602 (2003).
[21] R. C. Monreal, L. Guillemot, and V. A. Esaulov, J. Phys.: Condens. Matter **15**, 1165 (2003).
[22] Y. Bandurin, V. A. Esaulov, L. Guillemot, and R. C. Monreal, Phys. Rev. Lett. **92**, 017601 (2004).
[23] S. Wethekam and H. Winter, Surf. Sci. **596**, L319 (2005).
[24] S. Wethekam and H. Winter, Phys. Rev. Lett. **96**, 207601 (2006).
[25] S. Wethekam and H. Winter, Nucl. Instrum. Methods Phys. Res. B **258**, 7 (2007).
[26] H. H. Brongersma, M. Draxler, M. de Ridder, and P. Bauer, Surf. Sci. Rep. **62**, 63 (2007).
[27] D. Primetzhofer, S. N. Markin, J. I. Juaristi, E. Taglauer, and P. Bauer, Phys. Rev. Lett. **100**, 213201 (2008).
[28] A. Zwartkruis and T. Fonden, Surf. Sci. **290**, 134 (1993).
[29] R. Monreal and N. Lorente, Phys. Rev. B **52**, 4760 (1995).
[30] N. Lorente and R. Monreal, Surf. Sci. **370**, 324 (1997).
[31] M. A. Cazalilla, N. Lorente, R. D. Muiño, J.-P. Gauyacq, D. Teillet-Billy, and P. M. Echenique, Phys. Rev. B **58**, 13991 (1998).
[32] Diego Valdés, E. C. Goldberg, J. M. Blanco, and R. C. Monreal, Phys. Rev. B **71**, 245417 (2005).
[33] Diego Valdés, J. M. Blanco, V. A. Esaulov, and R. C. Monreal, Phys. Rev. Lett. **97**, 047601 (2006).
[34] W. More, J. Merino, R. Monreal, P. Pou, and F. Flores, Phys. Rev. B **58**, 7385 (1998).
[35] N. P. Wang, E. A. Garcia, R. Monreal, F. Flores, E. C. Goldberg, H. H. Brongersma, and P. Bauer, Phys. Rev. A **64**, 012901 (2001).
[36] S. Wethekam, Diego Valdés, R. C. Monreal, and H. Winter, Phys. Rev. B **78**, 075423 (2008).
[37] S. A. Cruz, E. Ley-Koo, and R. Cabrera-Trujillo, Phys. Rev. A **78**, 032905 (2008).
[38] R. Souda and M. Aono, Nucl. Instrum. Methods Phys. Res. B **15**, 114 (1986).
[39] S. Wethekam, Diego Valdés, R. C. Monreal, and H. Winter, Phys. Rev. B **78**, 033105 (2008).
[40] A. Fohlisch, P. Feulner, F. Hennies, A. Fink, D. Menzel, D. Sanchez-Portal, P. M. Echenique, and W. Wurth, Nature (London) **436**, 373 (2005).
[41] A. Duvenbeck, B. Weidtmann, O. Weingart, and A. Wucher, Phys. Rev. B **77**, 245444 (2008).
[42] R. Pfandzelter, Phys. Rev. B **57**, 15496 (1998).
[43] D. Gemmell, Rev. Mod. Phys. **46**, 129 (1974).
[44] D. J. O'Connor and J. P. Biersack, Nucl. Instrum. Methods Phys. Res. B **15**, 14 (1986).
[45] S. Wethekam and H. Winter, Nucl. Instrum. Methods Phys. Res. B **258**, 48 (2007).
[46] E. A. Garcia, N. P. Wang, R. C. Monreal, and E. C. Goldberg, Phys. Rev. B **67**, 205426 (2003).
[47] The values of the AN rates used in this work are the calculated ones assuming He on a hollow position, which reproduce the

experimental ion fractions in the survival regime (Ref. 36) better than the on-top rates used in Ref. 39. This produces the smaller factor of 1.2 by which the theoretical AN rates have to be multiplied to obtain perfect quantitative agreement with measured ion fractions, compared to the factor of 1.31 used in Ref. 39.

[48] L. A. Salmi, Phys. Rev. B **46**, 4180 (1992).

[49] Compared to the simulated distributions shown in Fig. 4, the statistics in Fig. 8 is slightly poorer which results in an increased scatter of data, especially for the angular distributions for outgoing ions in panels a and b. The scatter of data in the tails of the distributions has statistical origin.